Size Quantization and Electron Transport in Quantum Dots

Ashutosh Kumar Giri* Himanshu Kumar Pandey** Abhishek Ranjan Singh* Pramendra Ranjan Singh***
*Research Scholars, Deppt. of Physics, J.P. University, Chapra ,
**Principal, Shlokaa International School, Bhore-841426,
***Principal , Narayan College, GoriaKothi, Siwan

Abstract:- **Properties like color, melting point, ionization potential and electron affinity, electrical conductivity, or magnetism which for bulk amounts of matter do not depend on size become size-dependent when the size of a particle falls in at least one dimension below a certain limit, which is normally taken to be about 100nm. On this basis, the properties of matter can be tuned to their desired values by adjusting the size of nano particles and the thickness of thin layers or wires.The present paper aims to discuss the size quantization and electron transport in quantum dots. We started with the discussion with the properties of size quantization of nano crystals followed by the quantum size effects, surface effects and quantum tunneling besides discussions and illustrations of photo electrochemical and intensity-Modulated Photocurrent Spectroscopy.**

INTRODUCTION

A crystalline material which is size-restricted in three dimensions such that the electron wave functions are confined within its volume is called a quantum dot (QD). Due to this confinement the electronic properties of quantum dots depend on their size in the nanometer regime [1,2]. This effect, now called 'size-quantization', was first observed in 1926 with CdS colloids [3], but was only properly recognized in the 1980's [4,5]. Chemists and physicists have studied nanostructures extensively in the past two decades in order to understand the size-quantization effects in semiconducting and metal quantum dots.

Due to their extremely small sizes and their interesting electronic properties, quantum dots are promising building blocks for the fabrication of electronic and optoelectronic solid state devices. Integrated circuits (ICs) might be further miniaturized by using nano crystallites. The II–VI nanocrystals have a band gap which can be tuned in a broad range (up to 4 eV) by changing either their size or chemical composition; this makes them suitable candidates for applications as a Light Emitting Diode (LED) [6,7], a Single Electron Transistor (SET) [8-10], chromophores in solar cells [11-15], or as a 'building block' for photonic crystals [16]. Recently, a LED with an efficiency of 10 %, based on CdSe nano crystals in a semiconducting polymer matrix, was fabricated [17,18] The output color could be tuned in the entire visible range. A critical parameter for the performance of a SET, the principle of which is based on the Coulomb blockade effect, is the capacitance of the quantum dot, which is determined by its size. Quantum dots can be applied as stable fluorescent indicators in biological research; core-shell quantum structures of CdSe/ZnS have a very high luminescence quantum yield (up to100%). Since they can easily be attached to DNA [19] or proteins by a sulphide bond they can act as a luminescing label to monitor biological reactions. Semiconductor colloids can also be employed in photo catalysis; TiO_2 colloids irradiated with UV-light can photo-oxidize organic contaminants [20]. Methods for the preparation of large quantities of well-defined nanoparticles have been developed in order to study the size-quantization effect. A technique to grow low-dimensional structures, Molecular Beam Epitaxy (MBE), was developed at the end of the 1960's [22,23]. Arrays of quantum dots on substrates can be prepared by MBE or lithographic dry-etching [24-25]. Alternatively, quantum dots can be formed in the gas phase by laser vaporisation [25] or as colloids in suspension [27-28]. Chemists have succeeded in greatly improving the mono dispersity in size and shape of colloidal semiconductor quantum dots in the past decade [29]. High-quality suspensions can now be synthesized and the size distribution can be further narrowed by size-selective precipitation or photo etching [30-32].

Optical absorption and photoluminescence were first used to study the electronic structure of nanometer-sized semiconductor colloids. However, these techniques only provide information about the collective properties of large numbers of QDs and, due to a distribution in particle size, the luminescence signals are inhomogeneously broadened. With Scanning Probe Techniques such as Scanning Tunneling Spectroscopy (STM) and Scanning Near-field Optical Microscopy (SNOM), electrical and optical measurements on individual particles can be performed, avoiding problems arising from polydispersity. In the work described in this thesis the optoelectronic properties of semiconductor quantum dots, and charge transfer between such structures and a conducting substrate were studied in a novel way. For this purpose, metal substrates were provided with a (sub) monolayer of quantum dots; the optoelectrical properties of the systems were investigated with time-resolved photoelectron chemistry. The electronic structure of individual nanocrystals was investigated by Scanning Tunneling Spectroscopy at room temperature and at 4 K. This chapter presents an introduction to the size-quantization effect in semiconductors and electron transfer between a metal and a semiconductor quantum dot. In the latter sections the principles of the measuring techniques are explained and an outline of this thesis is given.

1.2 Size-quantization in Semiconducting Nanocrystals
1.2.1 Energy Bands in Bulk Semiconductor Crystals

To discuss the origin of energy bands in bulk semiconductors and electron tunneling between two systems, a single electron in a crystal is considered [33] The time-independent Schrödinger equation for an electron can be written as,

$$-\frac{\hbar^2}{2m_e}\nabla^2\Psi(x,y,z)+U(x,y,z)=E\Psi(x,y,z)$$ (1.1)

where m_e is the mass of the free electron, E is the kinetic energy, and $\nabla^2=\left(\frac{\partial^2}{\partial x^2}+\frac{\partial^2}{\partial y^2}+\frac{\partial^2}{\partial z^2}\right)$. In the free-electron

approach, the potential energy of the electron due to the crystal lattice of core ions $U(x,y,z)$ is neglected, and is taken as a constant (e.g. $U(x,y,z)=0$). In that case the solution of equation (4.1) for $\Psi(x,y,z)$ can be denoted as,

$$\Psi_{\vec{k}}(\vec{r})=\frac{1}{\sqrt{V}}e^{i\vec{k}.\vec{r}}$$ (1.2)

where $\vec{r}$ is the position vector (x, y, z), and $\vec{k}$ is the wave-vector (k_x, k_y, k_z); the plane periodic k wave, $i_e\vec{k}.\vec{r}$, has a constant

amplitude in any plane perpendicular to $\vec{k}$, and is periodic along lines parallel to $\vec{k}$, with a wavelength $l=\frac{2\pi}{k}$. The prefactor

$\frac{1}{\sqrt{v}}$ is due to the normalization condition, which requires that the particle must be present in the sample volume V. The linear

momentum of the electrons is $\vec{p}=\hbar\vec{k}$ and the kinetic energy is given by,

$$E(\vec{k})=\frac{\hbar^2k^2}{2m_e}$$ (1.3)

The occupation of the electron levels is in accordance with the Pauli Exclusion Principle. At 0 K, all energy levels below the Fermi-energy (E_F) are occupied by two electrons of opposite spin. The occupation of electron energy levels under thermal equilibrium at T > 0 K can be derived from statistical thermodynamics. The probability that an energy level, E, is occupied by an electron is given by the Fermi-Dirac function,

$$f(E)\frac{1}{1+e^{(E-\mu_e)/k_BT}}$$ (1.4)

in which μ_e is the electrochemical potential (Fermi-level) and k_B the Boltzmann constant. The free electron model can be refined by taking the scattering of the electron waves by the periodic lattice potential energy $U(x,y,z)$ into account. The distance between the centers of the core ions in the x- direction is denoted as dx. The electrons with low energy have wavelengths much longer than dx; however, at higher energy there are free electrons with wavelengths obeying the condition for Bragg reflection,

$$\frac{\lambda_e}{2}\cong\frac{d_x}{q}$$ (1.5)

Due to Bragg scattering on the periodic lattice potential, propagation of these electrons will be prohibited in the x-direction and standing waves are formed. Two standing waves can be constructed by a linear combination of the waves travelling in the positive and negative.10
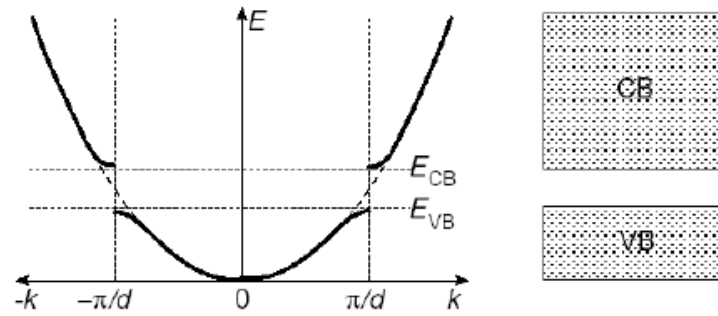
Figure 1.1 The formation of energy bands in a macroscopic semiconductor due to Bragg reflection of the electrons on the periodic lattice of the crystal.

X–directions. The electron density corresponding to the first standing wave is centered at the core ions, that of the second wave between the core ions. The two standing waves correspond to considerably different energies. The energy difference can be estimated by a perturbation method; it is equal to the periodic lattice potential in the x-direction. The scattering of the free electrons by the periodic lattice leads to discontinuities in the $E(k)$ relationship for k values at around $k = 2\dfrac{\pi}{d}$. These discontinuities lead to the formation of energy bands, separated by energy gaps, as presented in Figure 1.1. This derivation for the x-direction can be used in a similar way for the y and z-directions. The $E(k)$ relationship for free electrons is a good approximation for most of the electrons in a band, except for those near the edge of the Brillouin zones.

1.2.2 Quantum Size Effects

A (Wannier) exciton can be defined as the bound state of an electron-hole pair, which is due to a Coulomb interaction between the charge carriers [1]. The distance between the electron and the hole is the Bohr radius of the exciton, a_B, and is given by,

$$a_B = \frac{4\pi\varepsilon_0\varepsilon_\infty\hbar^2}{m_0 e^2}\left(\frac{1}{m_e^*} + \frac{1}{m_h^*}\right) \tag{1.6}$$

in which m^* and m^* are the effective electron and hole masses, respectively, and ε_∞ is the high- frequency relative dielectric constant of the medium. The resulting Bohr radius is much larger than that of a hydrogen atom, since the effective masses are considerably smaller than the mass of the electron at rest, m_0, and ε_∞ is considerably larger than 1. Values for a_B for the common semiconductors are in the range 10-100Å.

Nanocrystals have crystalline order and dimensions corresponding to some tens of a lattice constant in each direction. Electron scattering with the lattice leads to band formation, as for macroscopic crystals. However, the free electron wavelength and the Bohr radius can be comparable to or even larger than the crystal dimensions. This means that the nanocrystal acts as a quantum box for quasiparticles. The symmetry of the box is important for the solution of the Schrödinger equation. In the literature, a spherical symmetry is often used. For simplicity, we consider a rectangular box of dimensions L_x, L_y, and L_z surrounded by infinitely high energy walls. Stable solutions of the Schrödinger equation are standing waves. For instance in the x-direction, the free-electron and free-hole standing waves must fulfill,

$$L_x = n_e \times \frac{\lambda_e}{2} \quad (n_e = \pm1, \pm2, ...) \tag{1.7}$$

$$L_s = n_h \times \frac{\lambda_h}{2} \quad (n_h = \pm1, \pm2, ...) \tag{1.8}$$

From equations (1.5), (4.7) and (4.8) it follows that size quantization in the x-direction gives discrete k_x values for the electrons and holes. The total number of discrete states depends on the well width and depth. In the case of walls with a finite height, the wave function does not vanish at the edge of the well, but decays exponentially in the classically forbidden region. Therefore, the probability of finding a particle inside the well is always less than unity and decreases with increasing E_n. As a result of the reduced number of states and the confinement of the electron wave functions, a part of the $E(k)$ curve is replaced by discrete points as shown in Figure 1.2.

Brus has modeled electron confinement in a spherical box by using the effective mass approximation [5,34]. When $R \ll a_B$ the confined electron and hole have no bound state as in the definition of an exciton given above and the Coulomb interaction may be ignored to a first approximation. The mathematical treatment is similar to that for an electron in the spherical

potential well of a nucleus [35]. The state of the system is characterized by three quantum numbers, namely the principal number n, the orbital number l, and the magnetic number m. The states corresponding to different l values are denoted as s-, p-, d-, and f- states. Each state with a given l value has a $(2l+1)$ degeneracy, corresponding to m= 0, $\pm 1, \pm l$. For a spherically symmetrical potential box with an infinite barrier, the resulting energy of the exciton can be written as follows,
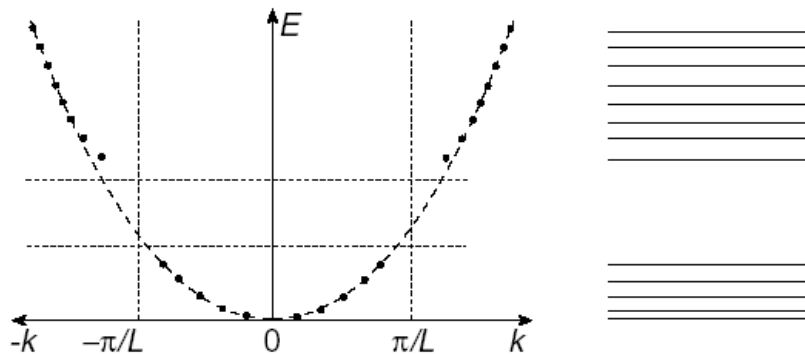

Figure 1.2 Due to the size-confinement of the semiconductor nanocrystal only the electron wave functions obeying R=nλ/2 can form standing waves; this and the reduced number of states lead to the formation of discrete energy levels instead of energy bands.

$$(1.9)$$

$$E_{nl} = E_g + \frac{\hbar^2 \chi_{nl}^2}{2m_0 R^2}\left(\frac{1}{m_e^*} + \frac{1}{m_h^*}\right)$$

in which E_g is the band gap of the macrocrystalline semiconductor, defined as the energy needed to excite an electron from the top of the valance band to the bottom of the conduction band. χ_{nl} is the nth root of the spherical Bessel function and l the order of the function; for l=0 (so-called s- states)$\chi_{n0}=\pi_n$. Weakly quantized quantum dots (with $R \sim a_B$) contain a large number of atoms and unit cells; therefore Bragg reflection at the periodic lattice will lead to the formation of continuous energy bands. Only the levels at the top of the valence band and at the bottom of the conduction band, which correspond to the most delocalized electron wave function, will be discrete (see Figure 1.3 (b). Highly quantized semiconductor quantum dots are sometimes called artificial atoms because they exhibit a discrete optical spectrum determined by their size (see Figure 1.3 (c)).

The electron and hole, confined in a space with dimensions smaller than the Bohr radius of the exciton, cannot however be considered as independent particles; the Hamiltonian must be expanded by two-particle kinetic terms and the Coulomb and confinement potential. This leads in the Brus model to an expression for the energy of the ground state of the electron-hole pair($1s_e1s_h$ or first excited state),

$$E(1s_e\,1s_h) = E_g + \frac{\pi^2\hbar^2}{2m_0 R^2}\left(\frac{1}{m_e^*} + \frac{1}{m_h^*}\right) - A\frac{e^2}{4\pi\varepsilon_0\varepsilon_\infty R} \qquad (1.10)$$

in which the second term describes confinement and the third the Coulomb electron-hole interaction. The coefficient A corresponds to 1.786 for the $1s_e1s_h$ state and has values between 1.6 and 1.9 for other states.[36] Equation (4.10) implies that the gap between the filled valence band levels and the empty conduction band levels increases when the radius of the particle decreases. Due to the electron-hole Coulomb interaction, the measured optical band gap has a slightly lower energy than the 'actual' electronic band gap.
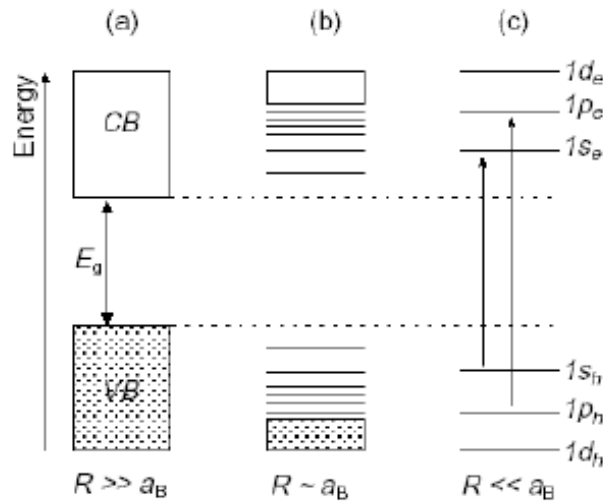
Figure 1.3 The effect of size on the electronic structure of a semiconductor crystal for three different size-ranges. (a) a macro crystalline semiconductor (R>>aB) with continuous energy bands; the filled valence band (VB) and empty conduction band (CB) and the band gap energy (Eg) are shown. (b) Semiconductor nanocrystal with a weak size-quantization (R~a_B). (c) Highly quantized dot (R<<a_B)with discrete atomic-like energy levels and optical transitions.
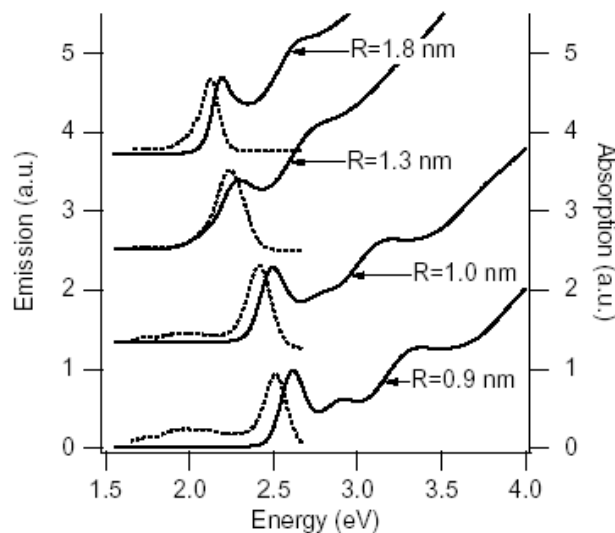

Figure 1.4 Absorption (solid lines) and emission (dotted lines) spectra of colloidal CdSe quantum dots, showing that the absorption edge shifts towards higher energies with respect to bulk CdSe (1.84eV) and that discrete energy bands become more pronounced as the particle size decreases.

The increase of the band gap and the transition from continuous energy bands to discrete energy levels upon a decrease of particle size has been observed by optical absorption spectroscopy in many colloidal semiconductor systems [30,37]. The absorption and emission spectra of colloidal CdSe quantum dots of different sizes studied in this work (see Figure 4.4) demonstrate these effects. Upon a decrease of the particle radius, the onset of the absorption and the emission maximum shift towards higher energies. A clear structure in the absorption spectra is observed for the smallest particles, corresponding to discrete optical transitions.

1.2.3 Surface States

Although the presence of surface states is by no means a size-quantization effect, surface states become increasingly important as the size of a structure reduces; the ratio of the number of surface to bulk atoms, which increases with decreasing particle radius, is very large for quantum dots. Surface atoms give rise to electron levels of energy different from those of the bulk levels; these levels can play an important role in light absorption and emission.[38] The importance of surface states in the photoexcited decay dynamics has become clear from time-resolved luminescence spectroscopy on colloidal suspensions of quantized PbS, CdS, CdSe, ZnO, and InP [39-42]. Besides direct conduction-to-valence band recombination, a broad band at

lower energy is often observed in emission spectra [37]; this sub-band gap emission can correspond to a transition either from the conduction band to a band gap state, or from a band gap state to the valence band. Alternatively, surface states can provide pathways for non-radiative recombination and therefore decrease the luminescence quantum yield. Charge carriers can also be trapped in deep band gap states, forming a long-lived excited state of lower energy [43].

1.3 Electron Tunneling

1.3.1 Basic Principles of Electron Tunneling

Metals and semiconductors generally have a high potential energy barrier at their surface, which confines the electrons within the solid [44]. At room temperature thermally activated escape of the electrons over the surface barrier is very improbable. However, quantum mechanical tunneling can occur when the interfacial barrier is very thin. This is the main mechanism of electron transfer through an insulating barrier between two solids in intimate contact.

$$-\frac{\hbar^2}{2m_e}\frac{\partial^2}{\partial x^2}\Psi(x) + E_{vac}\Psi(x) = E(x)\Psi(x) \qquad (1.11)$$

The free electron model discussed in section 1.2 allows a more quantitative discussion of the probability of finding an electron in a limited region just outside a crystal. The potential energy in the crystal is set to zero, and that of an electron at rest outside the crystal to E_{vac}. The Fermi-energy of the electrons in the crystal is considerably below E_{vac}; The work function, $E_{vac}-\mu_e$, is generally of the order of a few eV. The Schrödinger equation for a single free electron in the region outside the crystal for the x-direction is given by, The energy of the electron at rest in vacuum is larger than the total energy $E(x)$ of the impinging electron. A solution of equation (1.11) is,

$$\Psi_{vac}(x) = \frac{1}{\sqrt{L}}e^{-k_{vac}x} \qquad (1.12)$$

where x is the distance from the surface and k_{vac} the decay parameter in the x-direction

$$K_{vac} = \left[\frac{2m_e(E_{vac}-E(x))}{\hbar^2}\right]^{1/2} \qquad (1.13)$$

The wave function of an electron impinging on a surface wall decays exponentially outside the metal. The decay length $1/\kappa_{vac}$ depends on the effective barrier height $E_{vac}-E(x)$. Tunneling of an electron between two solid phases can occur if these phases are separated by a distance of the order of $1/\kappa_{vac}$. The probability of tunneling is relatively small when $x > 1/\kappa_{vac}$ (strong attenuation), and is then given by,

$$T = T_0 e^{-2\kappa_{vac}d} \qquad (1.14)$$

The distance dependence of the tunneling probability is determined by the exponential term, since the prefactor depends only weakly on the effective barrier height. Electrons close to the Fermi-energy which fulfill the condition $k_x^2 \gg k_y^2 + k_z^2$ have the highest tunnel probability for a barrier width, d. The rate constant for electron tunneling, *i.e.* the number of tunneling events per electron level per second, can be defined as,

$$k = k_0 e^{-\beta d} \qquad (1.15)$$

in which k_0 is the maximum number per second for $d \rightarrow 0$, and β is equal to $2\kappa_{vac}$. A typical value of β for an effective barrier height of 1 eV is 1.0 Å^{-1}. A change of 1 Å in the barrier width typically leads to a change of the tunneling rate by a factor 2.71. This extreme sensitivity of the tunneling rate to the barrier width forms the basis for the Scanning Tunneling Microscope (STM), developed in 1982 [45]. Already in 1922 field emission from metals was observed [46] and since 1937 the Field-Emission Microscope (FEM) has been used to study electron tunneling and the surface structure of metals [47]. Since 1960 electron tunneling was studied with planar metal / insulator (vacuum)/metal junctions [48,49].

1.3.2 Electron Tunneling between a Quantum Dot and a Metal

Colloidal semiconductor quantum dots can be adsorbed on a metal electrode by Vander Waals interactions of the capping molecules, which stabilize the dots in the suspension, with the metal surface. Alternatively, covalent anchoring of the dots to the metal is possible with a difunctionalised Self-Assembled Monolayer (SAM) [50-55].In addition, QDs can be grown electrochemically on a conductive substrate; the particle size can be controlled by the charge used to electrodeposit the dots [56-58].

A metal coated with a (sub)monolayer of nanocrystals can be used as working electrode in a conventional electrochemical cell. With such electrodes we have performed time-resolved photo electrochemistry. The metal electrode, coated with a monolayer of dots, can be considered as a 2D array of mutually independent Double-Barrier Tunnel Junctions (DBTJ). The junctions are formed between the metal substrate and the dot and between the dot and the electrolyte. Using a modulated light intensity it is possible to measure the rate of photoinduced tunneling between the dots and the metal or the electrolyte solution.

With Scanning Probe techniques it is possible to perform electrical measurements on individual quantum dots. When the STM tip is positioned above a dot a DBTJ is formed consisting of the metal/dot and dot/tip junctions [64-67]. A schematic illustration of the Double- Barrier Tunnel Junction is shown in Figure 1.5 (a) for an electrical and (b) for an electrochemical configuration, and in (c) the electrical circuit of the DBTJ for both configurations is shown. The electronic properties of individual semiconductor (and metal) particles have been investigated in this way with Tunneling Spectroscopy (TS).
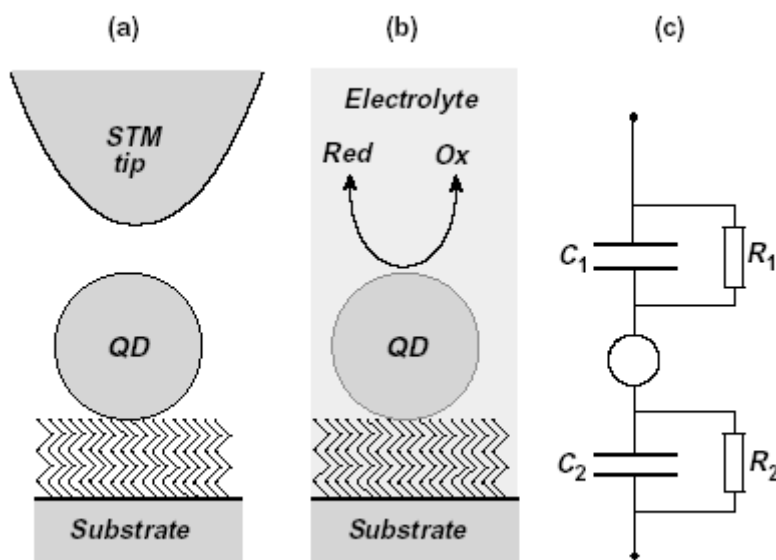

Figure 1.5 Schematic representation of a quantum dot on a Self-Assembled Monolayer on a metal substrate in (a) an electrical setup, with the STM tip as second electrode, and (b) in an electrochemical configuration, in which the electrolyte establishes the contact with the counter electrode. In (c) the electrical equivalent circuit of the Double-Barrier Tunnel Junction is shown for the two configurations.

1.3.3 Photoelectrochemical Measurements

The processes involved in photoinduced electron tunneling between a quantum dot and a metal electrode, forming the basis of the photo electrochemical and electrical measuring techniques, are presented in this and the following section.

Figure 1.6 shows a quantum dot on a metal electrode. An electron has been excited from a valence band level (HOMO) to a conduction band level (LUMO) of the quantum dot upon absorption of a photon ($hv>E_g$). Direct band-band recombination is usually very fast (~ps) and returns the system to the ground state. However, trapping of the hole or the electron in a band gap state may compete with the fast relaxation to the ground state. As a result, an excited state of lower energy is formed. It will become clear in this work that such a photoexcited state can possess a long lifetime, so that photoinduced tunneling between the dot and the metal can occur.

Resonant tunneling of the photoexcited electron to the metal is only possible when the substrate Fermi level ($E_{F,sub}$) is below the electron level (E_e), and an electron can only tunnel from the metal to the unoccupied level in the dot when the metal Fermi level is above this level (E_h). Thus, relaxation of the excited state to the ground state via photoinduced tunneling to and from the metal can only occur when $E_h<E_{F,sub}<E_e$. Decay of the photoexcited state via the metal can be observed by time-resolved measurement of the current in the external electrical circuit. When $E_{F,sub}$ is scanned and the photoinduced tunneling currents are measured in the external circuit, the electronic levels of the long-lived excited state can be resolved. The rate constants of these
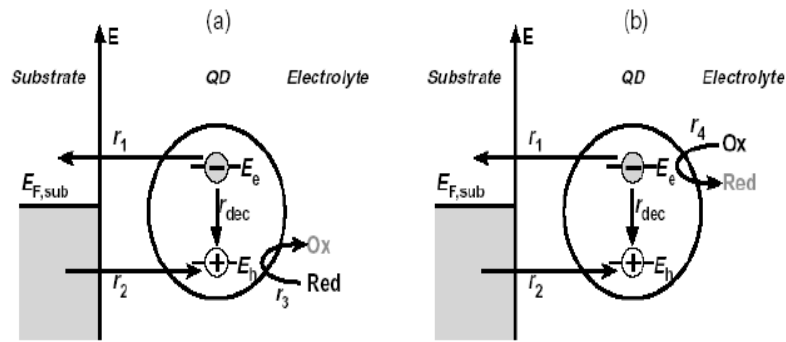
Figure 1.6 A photoexcited quantum dot adsorbed on a metal electrode, forming a DBTJ. After a photon is absorbed, one of the charge carriers is trapped in a localized state. (a) A hole scavenger is added to the electrolyte; when r_1 is followed by r_3 a steady-state anodic photocurrent is observed. (b) An electron scavenger is added; when r_2 is followed by r_4 a steady-state cathodic photocurrent is measured.

Tunneling processes may be determined by using time-resolved photoelectrochemistry. This technique will be explained in section 1.4. In the presence of either a reducing agent (Figure 1.6(a)) or an oxidizing agent (Figure 1.6(b)), electron transfer may also occur between the dot and the electrolyte. When r_1 is followed by r_3, a steady-state anodic photocurrent will be observed. Otherwise, when r_2 is followed by r_4, a steady-state cathodic photocurrent results.

1.3.4 Electrical Measurements with a Substrate/Dot/Tip Configuration

Figure 1.7 shows an energy level scheme for a highly quantized semiconductor quantum dot (with discrete energy levels) in contact with a metal substrate. By positioning the STM tip above the particle a DBTJ is formed. For simplicity, we assume that $E_{F,sub}$ is fixed with respect to the energy levels in the quantum dot. At small bias ($\Delta E \ll E_g$) the Fermi levels of the tip and the substrate are located in the bandgap of the nanocrystal and resonant electron tunneling via energy levels of the dot cannot occur. If a bias potential is applied such that $E_{F,tip} > E_{F,sub}$, resonant tunneling of an electron from the tip to the dot and from the dot to the substrate can occur when $E_{F,tip}$ reaches the first discrete conduction band level of the quantum dot. When $E_{F,tip}$ is raised further and reaches the next level, tunneling through this level can also take place. At a bias such that $E_{F,tip} < E_{F,sub}$ an electron can tunnel from the substrate to tip, via the levels of the valence band. In the current-bias plot a zero current range around $\Delta E = 0$ will be found, corresponding to the bandgap of the quantum dot. Steps in the current-bias (*I-V*) plot or peaks in the conductance-bias plot (*dI/dV-V*) will appear at bias values corresponding to resonant tunneling through discrete
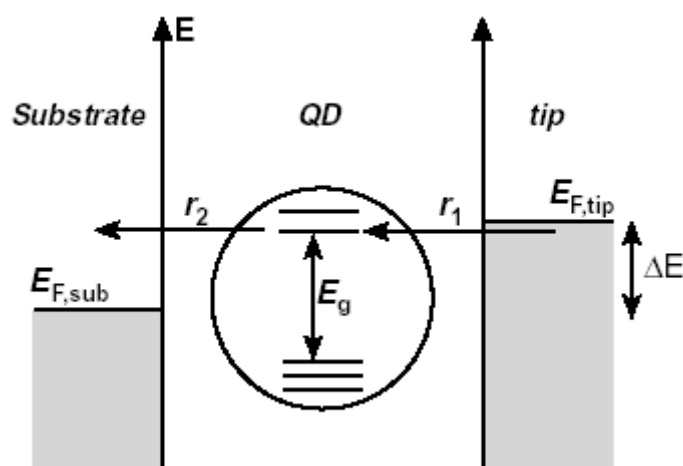

Figure 1.7 A schematic representation of a DBTJ for a metal/dot/tip configuration. Resonant tunneling via a discrete energy level in the quantum dot can occur when $E_{F,tip}$ reaches that level. Energy levels of the quantum dot. For an unambiguous assignment of the peaks in the dI/Dv vs V curve, it is necessary to have an asymmetrical DBTJ, such that $E_{F,sub}$ is locked to the energy levels of the quantum dot. Furthermore, Tunneling Spectroscopy using an electrostatic gate electrode or a magnetic field can be very helpful in elucidating the electronic structure of semiconducting quantum dots [68-69].

1.4 Intensity-Modulated Photocurrent Spectroscopy

Intensity-Modulated Photocurrent Spectroscopy (IMPS) is a time-resolved optoelectrical method. In this work the technique is used in a photoelectrochemical context to determine the rate constants of electron tunneling processes between the semiconductor quantum dots and a metal or redox system in the solution. IMPS has previously been used to study recombination processes, majority carrier injection at the bulk semiconductor/electrolyte interface [70], and charge transport in nanoporous semiconductor electrodes [71-72]. In this section the principle of the technique will be briefly described.

In IMPS, a small sinusoidal modulation, $\Phi(\omega)$, is superimposed on a steady-state light intensity, Φ, giving a photocurrent which also has a sinusoidal contribution ($\omega$is the modulation frequency). The modulated photocurrent $j(\omega)$ is measured using frequencies,ω, lower than $(RC)^{-1}$. The ratio $j(\omega)/e\Phi(\omega)$ is called the optoelectrical transfer function. Slow processes contributing to the total photocurrent will lead to a phase shift, $\theta(\omega)$, between$\Phi(\omega)$ and $j(\omega)$. The transfer function, determined by the amplitude ratio and the phase shift, can be plotted in the complex plane (imaginary component vs real component) or in a Bode plot (imaginary or real component vs frequency). In the experimental set-up used here, consisting of an illuminated metal/QD working electrode, the frequencies at which the imaginary part of the function shows
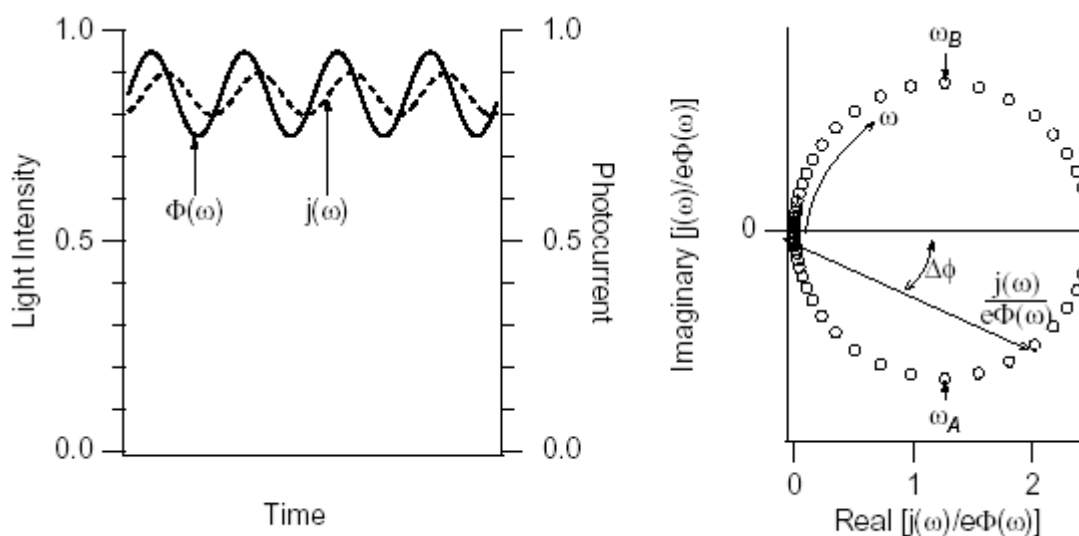

Figure 1.8 The principle of IMPS. (a) Modulated light intensity and photocurrent as a function of time. The modulation depth is ~10% of the base light intensity. (b) Complex plane plot of the recombination process of a photoexcited state in a semiconductor quantum dot adsorbed on a metal electrode via the metal. ω_A and ω_B correspond to the rate constants of the anodic and cathodic electron tunneling processes, respectively.

an extremum correspond to the rate constants of the photoinduced electron transfer between the QD and the metal, or the redox species in the electrolyte. In Figure 1.8 the optoelectrical transfer function, which might be expected for the decay of a photoexcited state in the quantum dot via the metal, is shown in the complex plane with the frequency as a parameter. In the high frequency limit electron transfer is slower than the light modulation, and both the real and imaginary components are zero. When the frequency is decreased, the phase shift between $\Phi(\omega)$ and $j(\omega)$ decreases, and a signal is observed. The frequency at the minimum of this semicircle, ωA, corresponds to the rate constant for electron tunneling from the dot to the gold, since the real component is anodic. When the frequency is further decreased a semicircle in the positive-positive quadrant is observed. The frequency at the maximum of this semicircle, ωB, corresponds to electron tunneling from the gold to the unoccupied level in the dot. In the low frequency limit the function is zero, meaning that both transfer from the QD to the metal and from the metal to the QD can follow the light modulation.

REFERENCES

[1]   S.V. Gaponenko, *Optical Properties of Semiconductor Nanocrystals***1998**, Cambridge University Press, United States of America
[2]   MRS Bulletin, february**1998**
[3]   G. Jaeckel, *Z. Tech. Phys.* **1926**, *6*, 301
[4]   A. Henglein, *J. Phys. Chem.* **1982**, *86*, 2291-2293
[5]   L.E. Brus, *J. Chem. Phys.* **1984**, *80*, 4403
[6]   H. Mattoussi, L.H. Radzilowski, B.O. Dabbousi, D.E Fogg, R.R. Schrock, E.L. Thomas, M.F. Rubner, and M.G. Bawendi, *J. Appl. Phys.* **1999**, *86*, 4390
[7]   Y. Yang, S. Xue, S. Liu, J. Huang, and J. Shen, *Appl. Phys. Lett.* **1996**, *69*, 377

[8]   D.L. KLein, P.L. McEuen, J.E. Bowen Katari, R. Roth, and A.P. Alivisatos, *Appl. Phys.Lett.* **1996**, *68*, 2574

[9]   M.A. Kastner, *Nature* **1997**, *389*, 667

[10]   D.L.KLein, R. Roth, A.K.L. Lim, A.P. Alivisatos, and P.L. McEuen, *Nature* **1997**, *389*,699.

[11]   H. Weller, *Advanced Materials* **1993**, *5*, 88

[12]   J. Fang, J. Wu, X. Lu, Y. Shen, and Z. Lu, *Chem. Phys. Lett.* **1997**, *270*, 145

[13]   S. Kohtani, A. Kudo, and T. Sakata, *Chem. Phys. Lett.* **1993**, *206*, 166

[14]   C. Nasr, P.V. Kamat, and S. Hotchandani, *J. Electroanal. Chem.* **1997**, *420*, 201

[15]   D. Liu, and P.V. Kamat, *J. Phys. Chem.* **1993**, *97*, 10769

[16]   Y.A. Vlasov, N. Yao, and D.J. Norris, *Advanced Materials* **1999**, *11*, 165

[17]   V.L. Colvin, M.C. Schlamp, and A.P. Alivisatos, *Nature* **1994**, *370,* 354

[18]   B.O. Dabbousi, M.G. Bawendi, O. Onitsuka, and M.F. Rubnar, *Appl. Phys. Lett.* **1995**, *66*,1316

[19]   A.P. Alivisatos, K.P. Johnsson, X. Peng, T.E. Wilson, C.J. Loweth, M.P. Bruchezjr, and P.G. Schultz, *Nature* **1996**, *382*, 609

[20]   D.F. Ollis, H. Al-Ekabi, Photocatalytic Purification and Treatment of Water and Air,Elsevier Science Publishers **1993**, Amsterdam, The Netherlands

[21]   C. Dekker, *Physics. Today* **1999**, *52*, 22

[22]   J.R. Arthur, *J. Appl. Phys.* **1968**, *39*, 4032

[23]   A.Y. Cho, *J. Vac. Sci. Technol.* **1971**, *8*, S31

[24]   D. Heitmann, and J P. Kotthaus, *Physics Today* **1993**, *june*, 56

[25]   M.A. Kastner, *Physics Today* **1993**, *january*, 24

[26]   U. Rothlisberger, W. Andreoni, M. Parinello, *Phys. Rev. Lett.* **1994**, *72*, 665

[27]   L. Spanhel, M. Haase, H. Weller, and A. Henglein, *J. Am. Chem. Soc.* **1987**, *109*,5649

[28]   M.L. Steigerwald, A.P Alivisatos, J.M. Gibson, T.D. Harris, R. Kortan, A.J. Muller, A.M. Thayer, T.M. Duncan, D.C. Douglas, L.E. Brus, *J. Am. Chem. Soc.* **1988**, *110*, 30460

[29]   X. Peng, L. Manna, W. Yang, J. Wickham, E. Scher, A. Kadavanich, and A.P. Alivisatos, *Nature* **2000**, *404*, 59-61

[30]   C.B. Murray, D.J. Norris, and M.G. Bawendi, *J. Am. Chem. Soc* **1993**, *115*, 8706

[31]   H. Matsumoto, T. Sakata, H. Mori, H. Yoneyama, *J. Phys. Chem. B* **1996**, *100*, 13781

[32]   A. van Dijken, A. Meijerink, D. Vanmaekelbergh, *Chem. Phys. Lett.* **1997**, *269*, 494

[33]   N.W. Ashcroft, and N.D. Mermin, *Solid State Physics* **1976**, Philadelphia

[34]   L.E. Brus, *J. Phys. Chem.* **1986**, *90*, 2555

[35]   P.W. Atkins, *Physical Chemistry* **1990**, Oxford University Press, Great Brittain

[36]   H.M. Schmidt, and H. Weller, *Chem. Phys. Lett.* **1986**, *129*, 615-618

[37]   A. Henglein, *Topics in Current Chemistry* **1988**, *143*, 115

[38]   A.P. Alivisatos, *J. Phys. Chem.* **1996**, *100*, 13226

[39]   A.J. Nozik, and O.I. Micic, *MRS Bulletin* february**1998**, 24

[40]   M. Kuno, J.K. Lee, B.O Dabbousi, F.V. Mikulec, and M.G. Bawendi, *J. Chem. Phys.*   **1997**, *106*, 9869

[41]   M.T. Nenadovic, M.I. Comor, V. Vasic, and O.I. Micic, *J. Phys. Chem.* **1990**, *94*, 6390

[42]   P. Guyot-Sionnest, and M.A. Hines, *Appl. Phys. Lett.* **1998**, *72*, 686

[43]   W.J. Albery, G.T. Brown, J.R. Darwent, and E. Saievar-Iranizad, *J. Chem. Soc. FaradayTrans. 1* **1985**, *81*, 1999

[44]   R. Wiesendanger, *Scanning Probe Microscpoy and Spectroscopy* **1994**, Cambridge University Press, Great Britain

[45]   G. Binnig, H. Rohrer, Ch. Gerber, and E. Weibel, *Phys. Rev. Lett.* **1982**, 49, 57

[46]   J.E. Lilienfeld, *Z. Phys.* **1922**, *23*, 506

[47]   E.W. Müller, *Z. Phys.* **1937**, *106*, 541

[48]   J. Bardeen, *Phys. Rev. Lett.* **1961**, *6*, 57

[49]   P.V. Gray, *Phys. Rev.* **1965**, *140*, A179

[50]   V.L. Colvin, A.N. Goldstein, and A.P. Alivisatos, *J. Am. Chem. Soc.* **1992**, *114*, 5221

[51]   J.E. Bowen Katari, V.L.Colvin, and A.P. Alivisatos, *J. Phys. Chem.* **1994**, *98*, 4109

[52]   S. Ogawa, F.F. Fan, and A.J. Bard, *J. Phys. Chem. B* **1995**, *99*, 11182

[53]   S. Ogawa, K. Hu, F.F. Fan, and A.J. Bard, *J. Phys. Chem. B* **1997**, *101*, 5707

[54]   M. Miyaki, H. Matsumoto, M. Nishizawa, T. Sakata, H.Mori, S. Kuwabata, and H.Yoneyama, *Langmuir* **1997**, 13, 742

[55]   S. Drouard, S.G. Hickey, and D.J. Riley, *Chem. Commun.* **1999**, *8*, 67

[56]   T. Nakanishi, B. Ohtani, K. Uosaki, *J. Phys. Chem .B* **1998**, *102*, 1571

[57]   G. Hodes, I.D.J. Howell, and L.M. Peter, *J. Electrochem. Soc.* **1992**, *139*, 3136

[58]   B. Alperson, H. Demange, I. Rubinstein, and G. Hodes, *J. Phys. Chem. B* **1999**, *103*, 4943

[59]   Y. Golan, G. Hodes, and I. Rubinstein, *J. Phys. Chem.* **1996**, *100*, 2220

[60]   Y. Kuk, M.F. Jarrold, P.J. Silverman, J.E. Bower, and W.L. Brown, *Phys. Rev. B* **1989**, *39*, 11168

[61]   R.H.M. Groeneveld, M.W.J. Prins, and H. van Kempen, *Surface Science* **1995**, *331-333*, 1299

[62]   B. Alperson, S. Cohen, I. Rubinstein, and G. Hodes, *Phys. Rev. B.* **1995**, *52*, R17017

[63]   T.D. Krauss, and L.E. Brus, *Phys. Rev. Lett.* **1999**, *83*, 4840

[64]   P.J.M. van Bentum, R.T.M. Smokers, and H van Kempen, *Phys. Rev. Lett.* **1988**, *60*, 2543

[65]   R.P. Andres, T Bein, M. Dorogi, S. Feng, J.I. Henderson, C.F. Kubiak, W. Mahoney, R.G. Osifchin, and R. Reifenberger, *Science* **1996**, *272*, 1323

[66]   C. Schönenberger, H van Houten, H.C. Donkersloot, A.M.T. van Putten, and L.G.J. Fokkink, *PhysicaScripta***1992**, *T45*, 289

[67]   67.   U. Banin, Y.W. Cao, D. Katz, and O. Millo, *Nature* **2000**, *400*, 542-544

[68]   L. Gurevich, L. Canali, and L.P. Kouwenhoven, *Appl. Phys. Lett.* **2000**, *76*, 384-386

[69]   D.C. Ralph, C.T. Black, and M. Tinkham, *Phys. Rev. Lett.* **1997**, *78*, 4087-4090

[70]   D. Vanmaekelbergh, A.R. de Wit, and F. Cardon, *J. Appl. Phys.* **1993**, *73*, 5049

[71]   P.E. de Jongh, and D. Vanmaekelbergh, *Phys. Rev. Lett.* **1996**, *77*, 3427

[72]   D. Vanmaekelbergh, F. Iranzo Marin, and J. van de Lagemaat, *Ber. Bunsenges. Phys. Chem.***1996**, *100*, 616

[73]   L.M. Peter, and D. Vanmaekelbergh, *'Advances in Electrochemical Science and Engineering'***1999**, John Wiley & Sons, Weinheim, Germany, 77